JACS
JOURNAL OF THE AMERICAN CHEMICAL SOCIETY
Article
pubs.acs.org/JACS

Selective Ag(I) Binding, H_2S Sensing, and White-Light Emission from an Easy-to-Make Porous Conjugated Polymer

Jie Liu,[†] Ka-Kit Yee,[†] Kenneth Kam-Wing Lo,[†] Kenneth Yin Zhang,[†,§] Wai-Pong To,[‡] Chi-Ming Che,[‡] and Zhengtao Xu*[,†]

[†]Department of Biology and Chemistry, City University of Hong Kong, 83 Tat Chee Avenue, Kowloon, Hong Kong, China
[‡]Department of Chemistry and HKU-CAS Joint Laboratory on New Materials, The University of Hong Kong, Pokfulam Road, Hong Kong, China

Supporting Information

ABSTRACT: Separating silver (Ag^+) from lead (Pb^{2+}) is one of the many merits of the porous polymer framework reported here. The selective metal binding stems from the well-defined chelating unit of N-heterocycles, which consists of a triazine (C_3N_3) ring bonded to three 3,5-dimethylpyrazole moieties. Such a rigid and open triad also serves as the distinct building unit in the fully conjugated 3D polymer scaffold. Because of its strong fluorescence and porosity (e.g., BET surface area: 355 m^2/g), and because of the various types of metal species that can be readily taken up, this versatile framework is especially fit for functionalization. For example, with $AgNO_3$ loaded, the framework solid exhibits a brown color in response to water solutions of H_2S, even at the dilution of 5.0 μM (0.17 ppm); whereas cysteine and other biologically relevant thiols do not cause notable change in color. In another example, tunable white-light emission was produced when an Ir(III) complex was doped (e.g., about 0.02% of the polymer weight) onto the framework. Mechanistically, the bound Ir(III) centers become highly emissive in the orange-red region, complementing the broad, bluish emission from the polymer host to result in the overall white-light quality: the color attributes of the emission are therefore easily tunable by the Ir(III) dopant concentration. With this exemplary study, we intend to highlight metal uptake as an effective approach to modify and enrich the properties of porous polymer frameworks and to stimulate interest in further examining metal−polymer interactions in the context of sensing, separation, catalyzes, and other applications.

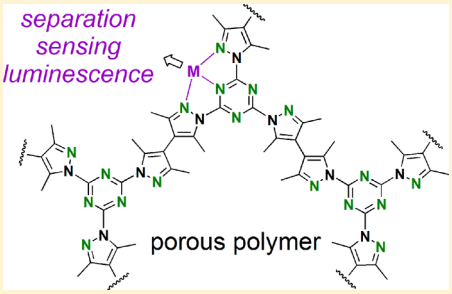

INTRODUCTION

Porous polymer frameworks (PPFs) as a growing class of advanced materials have been intensely studied owing to the salient advantages of stability and functionality.[1] The stability arises from the strong constituent covalent bonds that are often deployed in spatially confined and rigid configurations. Remarkable examples of this sort are seen in the covalent triazine-based frameworks (CTFs)[2] and the diamond-like networks based on tetraphenylmethane building blocks:[3] both systems withstand higher temperatures (e.g., 400 °C) and strong acid/base treatments, with stability of the former (i.e., CTFs) further highlighted in a recently reported application for electrochemical energy storage device, in which the CTF system continues to hold up after thousands of electrochemical cycles.[4] The functional versatility is rooted in the diverse modifications provided by organic chemistry and is further buttressed by the extraordinary stability of these covalent framework materials. Presently, the major thrust of the field is shifting from framework syntheses/pore characterization (e.g., via gas adsorption measurements) to the functionalization of the networks, in order to drive forward catalyzes,[1b,c,5] separation,[6] and other applications.[7]

One effective approach of functionalization is to integrate Lewis base donor groups into the framework structure, including N-heterocycle units,[5c,d,8] poly(thienylene arylene),[5e] Tröger's base,[9] Lin's binaphthol motif,[10] and isocyanurate.[5b] The importance of such groups is obvious. For example, they can be directly utilized as heterogeneous acid/base catalysts.[5f,11] Moreover, the donor groups often facilitate the uptake of metal species and thereby potentially enable within these novel porous mediums a much wider range of catalytic, photochemical, and photophysical processes. Among the numerous efforts to integrate donor units and to upload metal species into PPFs, the major intent is often focused on catalytic applications. By comparison, little has been reported on the use of PPFs for selective binding and separation of metal ions.

Here we report a PPF that, besides being able to selectively bind and separate Ag(I) ions from base metal ions (e.g., Pb^{2+}, Cd^{2+}, and so on; in aqueous solutions), offers multiple advantages. For example, the majority of Ag(I) can be readily extricated from the polymer matrix, thus enabling the recycling of the polymer host. The remainder (e.g., about 20%) of the Ag(I) species in the polymer host, on the other hand, can be used to detect and differentiate H_2S from other biologically relevant mercaptan molecules. Interestingly also, the conjugated

Received: October 30, 2013
Published: January 24, 2014

   dx.doi.org/10.1021/ja411067a | J. Am. Chem. Soc. 2014, 136, 2818−2824

polymer framework features distinct photoluminescent properties that can be easily tuned to generate white-light emission amid a wide range of other wavelength profiles. Let us start with the synthesis and design of this polymer framework.

RESULTS AND DISCUSSION

Convenient Synthesis. Both monomer building blocks are easy to obtain: 2,4,6-trichloro-1,3,5-triazine (i.e., cyanuric chloride, CC) is an industrial material, and 3,3′,5,5′-tetramethyl-4,4′-bipyrazol (TMBP, see Scheme 1) is available

Scheme 1. Synthetic Scheme for the TMBPT Polymer Framework[a]

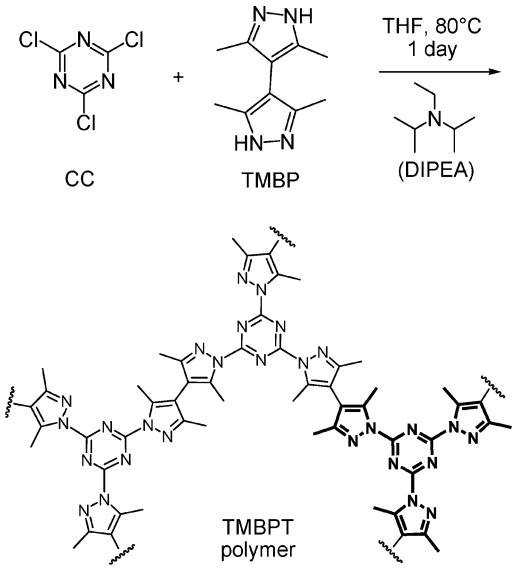

[a]Highlighted at lower right is a TPT unit.

commercially or from an inexpensive preparation using 2,4-pentanedione and hydrazine.[12] The assembly of the polymer framework simply involves refluxing a mixture of THF (tetrahydrofuran), CC, TMBP, together with the mild base *N*,*N*′-diisopropylethylamine (DIPEA) as a promoter/catalyst (see Scheme 1). The mild reaction requires no strong acid/base reagents and is especially compatible with industrial production. The metal-free procedure also obviates the toxicity and other detrimental effects of metal residues that often interfere with applications in medical and optical/electronic technologies.

The resultant TMBPT (the last T standing for triazine) polymer framework features the tritopic node of the triazine and its three dimethylpyrazole neighbors (i.e., the TPT unit as highlighted in Scheme 1). The relative rigidity of the TPT unit, together with the large torsional angle enforced by the methyl groups, is meant to promote the formation of a 3D open framework that contains significant void. The conjunction of triazine core and the pyrazole groups also creates distinct chelating motifs of the nitrogen donors for potentially effective binding of metal ions. In principle, two types of orientations are possible for the three pyrazole moieties in the TPT unit: one features three equivalent bidentate motifs (i.e., the lower left one in Scheme 1); the other is less symmetrical and contains the mono-, bi- and tridentate modes (the lower right one in Scheme 1). No effort was made to assess the ratio of the two configurations, but in either case, the chelating character is prominent.

The results of elemental analyses (e.g., of C, H, and N; EDX indicates no Cl remaining in the solid product of TMBPT, Figure S1) are consistent with the formation of the TMBPT framework (see SI). Thermogravimetric analysis (TGA, Figure S2) on the TMBPT powder reveals a stable weight region up to 300 °C, indicative of the nonvolatile, polymeric nature of the product; while the X-ray powder diffraction pattern exhibits three very broad peaks, suggesting a rather low degree of crystalline order of the TMBPT solid (Figure S3). The formation of the TPT core in the TMBPT polymer framework is also demonstrated by the synthesis of the triad molecule **M1** (Scheme 2) when excess TMBP (relative to CC) was used

Scheme 2. Molecule M1

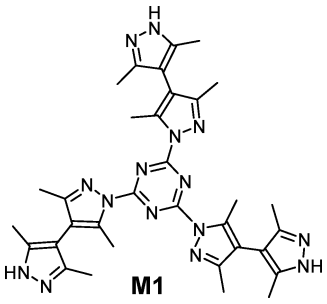

under similar reaction conditions (see Scheme S1). Also revealing is a comparison of the IR and Raman spectra of the TMBP reactant, the intermediate product **M1**, and TMBPT polymer (Figure 1). Most notably, the **M1** triad and the TMBPT shares a number of distinct features that are absent in the TMBP reactant, including: the peaks at 745, 812, 1095, and 1129 cm^{-1} in the IR spectra; the strong peak 990 cm^{-1} and the overall resemblance of the Raman spectra. Such similarities point to the common structural features between the **M1** molecule and the TMBPT polymer and are associated with the TPT/triazine core (as highlighted in Scheme 1). For example, the strong Raman peak at 990 cm^{-1} arises from the symmetrical ring deformation (C, N out of phase) of the triazine core, and the medium IR peaks at 1095 and 1129 cm^{-1} can be ascribed to the stretch of the C−N bonds off the triazine ring. The efficient reactions observed here are also in line with that of similar reactions between CC and amine molecules[13] as well as the near quantitative reaction between CC and the model compound 3,5-dimethylpyrazole (DMP, see Scheme S2 and Figure S4). In addition, the solid-state ^{13}C NMR measurement of the TMBPT sample also verifies the efficiency of the polymerization reaction. As seen in Figure S5, the aromatic region of the solid-state ^{13}C NMR spectrum of TMBPT is dominated by four distinct peaks (164.52, 152.63, 142.45, and 115.00 ppm) corresponding to the carbon signals of the polymer backbone, whereas a small peak found at higher field (106.66 ppm) can be assigned to the dangling, monoreacted TMBP units (as TMBP was added in slight excess relative to CC in the reaction).

Gas Sorption. CO_2 sorption experiments at 273 K (pressure range: from 8×10^{-3} to 780 mmHg) on the TMBPT sample (previously activated by Soxhlet extraction in methanol) revealed highly reproducible typical type-I gas adsorption isotherms (CO_2 gas, 273 K, Figure 2) with a Brunauer−Emmett−Teller (BET) surface area of 355 m^2/g. The validity of the BET model is also demonstrated by the linear fit of the data, as seen in the inset of Figure 2, and by the

dx.doi.org/10.1021/ja411067a | J. Am. Chem. Soc. 2014, 136, 2818−2824

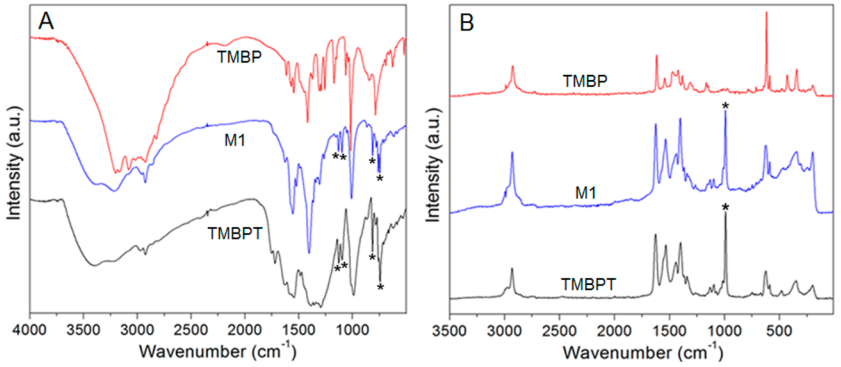

Figure 1. The IR (A) and Raman (B) spectra of TMBP, the **M1** molecule, and the TMBPT polymer. The stars mark selected peaks seen in both **M1** and TMBPT.

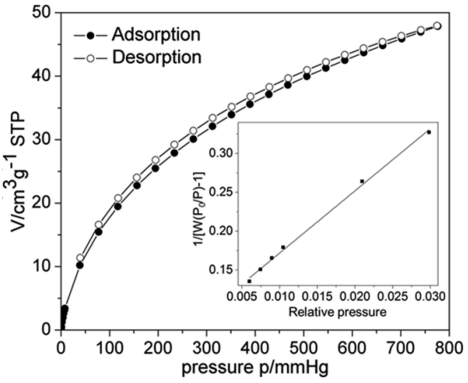

Figure 2. CO_2 sorption isotherm at 273 K for an activated TMBPT sample (126 mg, activated by evacuating at 120 °C for 12 h). Inset: the BET isotherm.

positive, reasonable C constant (C = 88), which is associated with the heats of adsorption (first layer) and condensation (multilayer). Monte Carlo analysis on pore size distribution and pore volume (Figure S6) of the CO_2 adsorption isotherms (273 K) indicated an average pore width of 0.48 nm and a modest micropore volume of 0.149 cm^3/g. The small pore size thus uncovered points to the importance of the micropore and ultramicropores in the structure, which could complicate porosity studies in certain cases (e.g., due to significant diffusion barriers).

One such case is the N_2 sorption experiments (e.g., at the much lower temperature of 77 K). Herein, adsorption at the micropore domain (i.e., at very low relative pressure) was not observed, indicating difficulty in accessing the very narrow micropores. Such a marked difference from the typical adsorption observed of CO_2 is often observed of microporous polymeric materials and has been well rationalized. First, CO_2 has a much higher saturation pressure P_0 (i.e., smaller relative pressure P/P_0) at 273 K, making it possible to investigate the microporosity at this higher temperature, where stronger thermal motion of the framework provides for faster diffusion and easier access of the pore regions. Also, the diffusion of CO_2 into micropores is facilitated by the following: CO_2 has a quadrupole moment and is more polarizable, thereby interacting more effectively with host material; CO_2 (0.33 nm) has a slightly smaller kinetic diameter than N_2 (0.364 nm).

The micropores and ultramicropores in this system also complicate the characterization of the mesoporous property (i.e., at higher relative pressures) based on N_2 sorption (at 77 K), because they tend to create the "bottlenecks" restricting access to the mesopores. The bottleneck effect is readily seen in one of the adsorption/desorption isotherms we obtained, wherein the distinct H2-type hysteresis loop corresponds to the delayed desorption caused by the blocking of the exit pathways (Figure S7).[14] The specific surface area (230 m^2/g) as well as the pore size/volume data (e.g., Figure S8) thus derived may therefore involve larger degree of uncertainty than systems of more regular porous features.

Aside from the gas sorption behaviors, porosity often expresses itself rather differently in other situations, e.g., in a solvent where swelling of the pores becomes significant and helps to open up the micropores and the bottlenecks to the mesopores. The importance of this effect has begun to be recognized even in metal−organic frameworks with well-ordered, crystalline structures.[15] As will be seen in the metalation processes described below, this effect is also especially pronounced for the flexible, organic TMBPT system featuring wide pore size distribution. On the other hand, typical gas sorption (e.g., BET curves) indicates open and accessible pores in vacuum, thus demonstrating the structural persistence and stability of the framework with regards to solvent/guest loss. Such so-called permanent porosity, however, does not always guarantee advantages, especially in solution-based applications. After all, many "permanent" pores (e.g., in MOFs) are readily degraded by moisture or other common reagents.

Effective Metal Uptake. In a typical run, the activated TMBPT solid (300 mg, equivalent to about 0.83 mmol of the TPT unit in Scheme 1) was placed in an aqueous solution containing excess $AgNO_3$ (495 mg, 2.91 mmol in 33 mL of water). After the mixture was stirred for 48 h at room temperature in the dark, the resultant solid (which remained yellowish) was separated by filtration and washed repeatedly by water (e.g., 10 × 10 mL, to remove residual unbound Ag^+ salts). CHN elemental analyses on the resultant solid sample found [C (38.73%), H (4.82%), N (23.98%)], while ICP indicated Ag content to be 15.6%. These elemental data can be fitted by the formula $(C_{18}H_{18}N_9)\cdot(AgNO_3)_{0.80}\cdot(H_2O)_{3.5}$ [calcd C (38.65%), H (4.50%), N (24.54%), Ag (15.43%)]. This formula indicates an ~0.8:1 $AgNO_3$/TPT molar ratio, and the Ag(I) uptake is thus found to be substantial, further demonstrating the open and porous nature of the bulk sample under the conditions. Uptake of other metal species is also possible. For example, $PdCl_2$ can be loaded to reach a 2.2:1 Pd/TPT ratio (see SI for details), a ratio that compares favorably with the pioneering system of Hatn-based (hexaazatrinaphthylene) network polymer reported by McKeown and co-workers.[8a] The effective Pd

dx.doi.org/10.1021/ja411067a | J. Am. Chem. Soc. 2014, 136, 2818−2824

loading in the TMBPT matrix shall facilitate future studies on the TMBPT polymer for potential applications in heterogeneous catalysis.

The Ag(I) and Pd(II)-loaded samples thus prepared become much weaker in photoluminescence, whereas the as-made sample features an intense, broad peak that comes off as whitish with a slight blue quality (Figure 3). The response of the

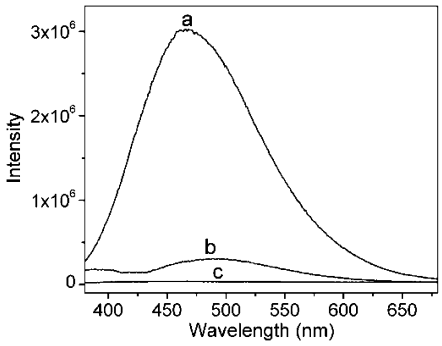

Figure 3. Room-temperature solid-state emission spectra: (a) activated TMBPT polymer, (b) $AgNO_3$-loaded TMBPT, and (c) $PdCl_2$-loaded TMBPT powders. The excitation wavelength λ_{ex} was 360 nm.

emission properties to metal guests is potentially useful for tuning the photoluminescent properties (see below for the white-light emission) and for monitoring the presence of metal species. As expected, CO_2 sorption (273 K, Figure S9) reveals a smaller specific surface area of 136 m^2/g for the Ag(I)-loaded TMBPT sample (cf. 355 m^2/g before Ag upload). Also the sorption isotherms feature a significant H2-type hysteresis, which, as discussed above, suggests aggravated bottleneck effects due to the loaded $AgNO_3$ further blocking the passage of the gas molecules.

The uploaded Ag species can be retrieved, and the TMBPT matrix can reused for additional cycles of metal uptake. For example, tetramethylthiourea (TMTU, Scheme 3), with its

Scheme 3. TMTU

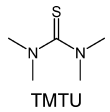

distinct sulfur donor, was found to be effective in stripping the Ag(I) species off the TMBPT matrix. Such stripping can be achieved by stirring the $AgNO_3$-loaded TMBPT solid (300 mg, prepared as mentioned above) in a water solution of TMTU (300 mg in 30 mL water) at 50 °C for 16 h in the dark. After the resultant solid was washed with water (about 200 mL) and THF (5 × 10 mL) to remove the residual TMTU, the Ag content was found by ICP to have dropped from 15.6% to 4.8%. Thus, the majority (e.g., 70%) of the loaded Ag(I) species can be extracted by the TMTU agent, which also serve to demonstrate the penetrable nature of the host matrix (e.g., with regard to TMTU as the guest). The cycle of upload and stripping can be repeated without significant compromise on the uptake and retrieval capabilities (see Table S1). For example, after the $AgNO_3$ was uploaded in the third round, the BET isotherm features remain little changed (surface area: 120 m^2/g, Figure S10), as compared with the $AgNO_3$-loaded sample in the first round.

Selective Ag(I) Uptake. Silver as a precious metal often naturally occurs in mineral forms together with ores of copper, nickel, zinc, and lead, and separation of Ag(I) from these base metal species is of great industrial importance.[16] Tests of selective Ag(I) binding are therefore especially meaningful for further exploring the applicability of TMBPT polymer system in separation science. For this, we first dissolve in water $AgNO_3$ and the following: $Cu(NO_3)_2{\cdot}3H_2O$, $Zn(NO_3)_2{\cdot}6H_2O$, $Co(NO_3)_2{\cdot}2H_2O$, $Cd(NO_3)_2{\cdot}4H_2O$, $Ni(NO_3)_2{\cdot}6H_2O$, and $Pb(NO_3)_2$. The concentration of each of the metal ions was set at about 50 ppm (see Table S2). An as-made TMBPT sample (50 mg, about 0.14 mmol of the TPT unit) was placed into 50 mL of the above mixture solution, which contains 2.6 mg (0.024 mmol) of Ag(I) and a total of 0.21 mmol of metal ions. In this test, the TPT units are set to decidedly outnumber the Ag(I) ions, so as to give other metal ions ample opportunity to access the TPT sites and to fully unveil the selectivity for the individual metal ions. The mixture was then stirred in the dark, and the solution of the mixture was sampled at different times (1, 3, 8, 19, 26, 44 h) for monitoring the concentrations of the metal species present in the solution.

The remarkable selectivity for Ag(I) is readily seen in the plot of Figure 4 and the data in Table S2. Within the first 8 h,

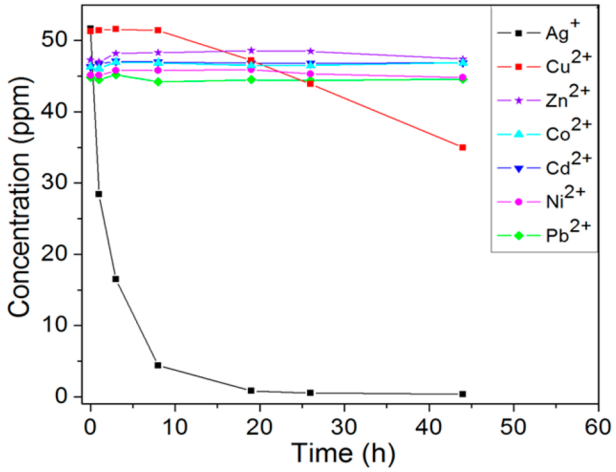

Figure 4. A plot of the concentrations (ppm) of the individual metal ions in a mixture solution at different hours after being mixed with TMBPT.

Ag(I) ion rapidly decreases in concentration, indicating efficient uptake by the TMBPT matrix, whereas concentrations of all other ions remain little changed. Specifically, by 8 h, over 90% of the Ag(I) ions in solution has been taken up by the TMBPT solid; later on at 44 h, the Ag(I) concentration was further reduced to 0.35 ppm (i.e., <1% of the original 52 ppm). Among the other ions, only Cu(II) exhibits significant decrease in concentration, but only after 8 h, and it remains above 35 ppm even at the 44 h (cf. the original being 51 ppm). The majority of the Cu(II) ions (about 70%) thus remain in solution; they are not taken up by TMBPT under the conditions. Of particular interest is Pb(II), because $PbCl_2$, like AgCl, is insoluble in water, which makes it impractical to separate the two by means of halide precipitation. The distinct selectivity of TMBPT for Ag(I) thus points to a convenient protocol for its separation from Pb(II). Generally speaking, the strong selective binding of Ag(I) is possibly driven by the higher (less negative) Gibbs free energy of hydration for silver ions than other metal

dx.doi.org/10.1021/ja411067a | J. Am. Chem. Soc. 2014, 136, 2818−2824

ions[16] as well as by the kinetics/liability of the coordination properties of Ag(I).

Detection of H_2S. The metal-laden, porous TMBPT polymer framework offers advantages for potential sensing applications. First, the porosity and large surface area of the solid-state matrix allow analytes to diffuse throughout the bulk and to fully access the anchored metal sites. Also, the anchoring of the metal centers (i.e., via the nitrogen coordination donors) is only moderate in strength, so that they remain potentially reactive/responsive upon being accessed by the guest analyte. The anchoring, on the other hand, is robust enough to prevent leaching and aggregation and thus to provide for better stability, e.g., the $AgNO_3$-loaded TMBPT is stable to water and does not turn black even after hours of exposure to light (unlike many light-sensitive silver salts).

As a preliminary test to exploit the nice balance of reactivity and stability in the solid state, we demonstrate here the highly sensitive colorimetric detection of H_2S in water. Most notably, even at rather low loading of Ag(I) (e.g., using a depleted sample after extraction by TMTU; with the $AgNO_3$/TPT ratio being about 1/5), a light but distinct brown coloring quickly developed even when the H_2S concentration was as low as 5.0 μM (0.17 ppm), as shown in Figure 5. At the higher

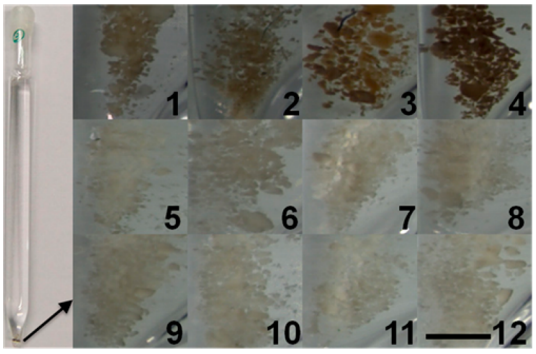

Figure 5. Photo images of the setup for the detection of H_2S (left) and of the $AgNO_3$-loaded TMBPT powder after being stirred for 4 h at 50 °C in: (1) 5 μM H_2S; (2) 10 μM H_2S; (3) 50 μM H_2S; (4) 100 μM H_2S; (5) 5 mM glutathione; (6) 5 mM cysteine; (7) 5 mM NaSCN; (8) 5 mM Na_2SO_3; (9) 5 mM $Na_2S_2O_3$; (10) Kpi buffer; (11) DI water; (12) 5 mM H_2O_2 solution. The scale bar is 0.80 mm.

concentrations of 10, 50, and 100 μM, the coloring becomes darker in a monotonic fashion, indicating the potential for colorimetric analysis. Moreover, the color change thus triggered is highly specific for H_2S. For example, biologically relevant thiols, such as glutathione and cysteine, and other reactive sulfur species (e.g., thiocyanate, sulfite, and thiosulfate, see Figure 5) do not cause any notable color change to the $AgNO_3$-loaded TMBPT powder even at the high concentration of 5 mM (i.e., over 1000 times the detection limit of H_2S). In particular, the water stability of the Ag-TMBPT solid is especially suited for the topical application of monitoring H_2S in physiological settings and in industrial waste/pollution control.[17]

Tuning for White-Light Emission. As previously demonstrated by Lo and others,[18] $Ir_2(pq)_4Cl_2$ (Scheme 4), which is nonemissive per se, can be rendered strongly emissive in the orange-red region, when the Cl atoms are displaced by nitrogen-based donor molecules. One implication here is obvious: by complementing the broad, bluish emission of the TMBPT polymer the orange-red features of the Ir(III) centers

Scheme 4. $Ir_2(pq)_4Cl_2$[a]

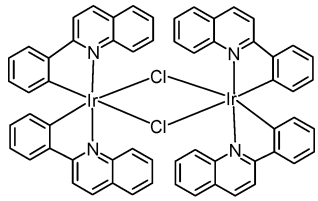

$Ir_2(pq)_4Cl_2$

[a]Bonds not drawn to scale.

(as being bound to the nitrogen donors on the TMBPT polymer host), one could potentially generate white-light emission, a property that is of great importance for the lighting industry.[19] Indeed, simply by stirring the TMBPT powder (e.g., 18.0 mg) and a dilute solution of $Ir_2(pq)_4Cl_2$ (e.g., 7.5 ppm in CH_2Cl_2, 1.0 mL, the Ir content being 0.02% of the polymer weight) for 15 min, one can effectively dope the Ir(III) complex into the TMBPT polymer host, and distinct white-light emissions were observed of the resultant solid sample (labeled as TMBPT-Ir-*a*). The white emission appears homogeneous throughout the powder sample (see the photo insets of Figure 6) and remains unchanged even after being repeatedly washed by CH_2Cl_2, indicating the robust and stable binding of complex $Ir_2(pq)_4Cl_2$ onto the TMBPT host.

The emission spectra of the pristine TMBPT polymer are shown in Figure 6. Overall, a longer excitation wavelength (λ_{ex}) tends to red-shift the emission maximum, e.g., with λ_{ex} being 320, 360, and 375 nm, the emission peaks at 455, 465, and 485

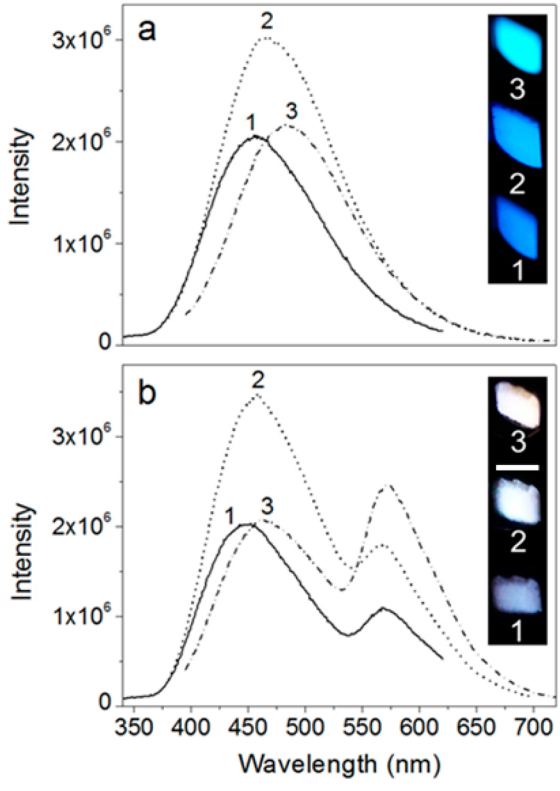

Figure 6. Room-temperature emission spectra of a pristine TMBPT powder (a) and the TMBPT-Ir-*a* powder (b). The excitation wavelengths for 1−3 are 320, 360, and 375 nm, respectively. The scale bar is 0.60 cm.

dx.doi.org/10.1021/ja411067a | J. Am. Chem. Soc. 2014, 136, 2818−2824

nm, respectively, with the corresponding CIE[20] coordinates of (0.18, 0.21), (0.19, 0.25), and (0.21, 0.31); all within the bluish region of the chromaticity graph (see Figure 7). Notice also

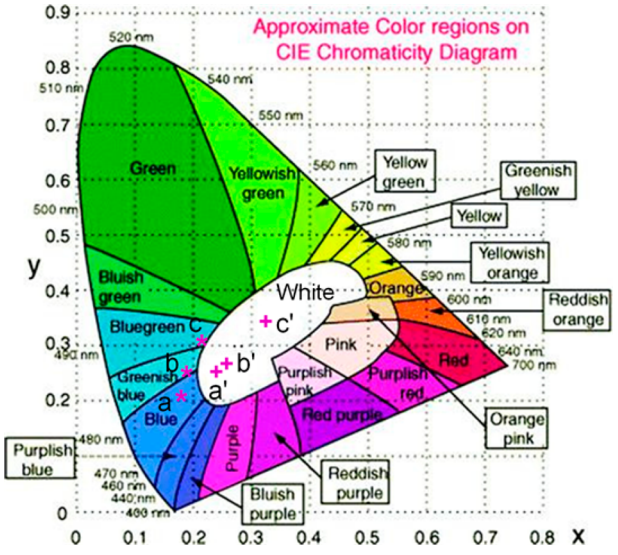

Figure 7. CIE-1931 chromaticity diagram and the positions for emissions of prisitne TMBPT [irradiated by 320 (a), 360 (b), and 375 nm (c)] and TMBPT-Ir-*a* [irradiated by 320 (a′), 360 (b′), and 375 (c′) nm] as marked by the stars and the crosses, respectively.

that the emission intensity is the greatest with λ_{ex} = 360 nm. For the doped polymer TMBPT-Ir-*a*, the emission maxima becomes less dependent on the excitation wavelengths: when excited at 320, 360, and 375 nm, respectively, the emission from the polymer host peaks at 445, 458, and 465 nm, whereas the new emission feature, arising from the Ir(III) moiety, remains at 570 nm for all three cases, and the corresponding CIE coordinates are now modified to be (0.24, 0.25), (0.25, 0.26) and (0.32, 0.34); all within the white-light region (see Figure 7) in the chromaticity graph. In general, the CIE coordinate as well as other aspects of the color quality of the emission can be conveniently tuned over a broad range by adjusting the concentration of the Ir(III) dopant in the polymer host. For example, when the Ir(III) content was raised to 0.04% (as in sample TMBPT-Ir-*b*), the emission from the Ir(III) centers becomes more significant, resulting in a stronger orange-red quality in the overall emission feature (e.g., see the top spectrum in panel 3B of Figure S11). Measurements on the powder samples of TMBPT, TMBPT-Ir-*a*, and TMBPT-Ir-*b*, using the integration sphere setup,[19u,21] indicate a fluorescence quantum efficiency on the order of 5−6%. Notice though that the integration sphere method tends to underestimate the actual value because of reabsorption of the emitted light by the sample.[21c,22] Overall, the quantum efficiencies found here are similar to a rare-earth-doped MOF reported by Chen and co-workers,[19d] while comparing favorably with a white-emitting nanocrystal sample of CdSe.[23]

■ ASSOCIATED CONTENT

Supporting Information

Additional experimental procedures, X-ray powder diffraction pattern of TMBPT, sorption isotherms and related graphs, detailed procedures for quantum yield measurement. This material is available free of charge via the Internet at http://pubs.acs.org.

■ AUTHOR INFORMATION

Corresponding Author

zhengtao@cityu.edu.hk

Present Address

[§]Key Laboratory for Organic Electronics & Information Displays and Institute of Advanced Materials, Nanjing University of Posts and Telecommunications, Nanjing 210023, China

Notes

The authors declare no competing financial interest.

■ ACKNOWLEDGMENTS

This work is supported by City University of Hong Kong (projects 7002723 and 7008095). Z.X. acknowledges the Alexander von Humboldt Foundation for a Humboldt Research Fellowship for Experienced Researchers (host: Prof. M. Antonietti). We thank Prof. Cheng Wang and Ms. Huimin Ding of Wuhan University (College of Chemistry and Molecular Sciences) for conducting the ^{13}C solid-state NMR study on TMBPT.

■ REFERENCES

(1) (a) Kaur, P.; Hupp, J. T.; Nguyen, S. T. *ACS Catal.* **2011**, *1*, 819. (b) Zhang, Y.; Riduan, S. N. *Chem. Soc. Rev.* **2012**, *41*, 2083. (c) Xie, Z.; Wang, C.; de Krafft, K. E.; Lin, W. *J. Am. Chem. Soc.* **2011**, *133*, 2056. (d) Dawson, R.; Laybourn, A.; Clowes, R.; Khimyak, Y. Z.; Adams, D. J.; Cooper, A. I. *Macromolecules* **2009**, *42*, 8809. (e) Xiang, Z.; Cao, D. *J. Mater. Chem. A* **2013**, *1*, 2691. (f) McKeown, N. B.; Budd, P. M. *Macromolecules* **2010**, *43*, 5163. (g) Thomas, A. *Angew. Chem., Int. Ed.* **2010**, *49*, 8328. (h) Ben, T.; Qiu, S. *CrystEngComm* **2013**, *15*, 17.

(2) (a) Kuhn, P.; Antonietti, M.; Thomas, A. *Angew. Chem., Int. Ed.* **2008**, *47*, 3450. (b) Kuhn, P.; Thomas, A.; Antonietti, M. *Macromolecules* **2009**, *42*, 319. (c) Ren, S.; Bojdys, M. J.; Dawson, R.; Laybourn, A.; Khimyak, Y. Z.; Adams, D. J.; Cooper, A. I. *Adv. Mater.* **2012**, *24*, 2357. (d) Katekomol, P.; Roeser, J.; Bojdys, M.; Weber, J.; Thomas, A. *Chem. Mater.* **2013**, *25*, 1542.

(3) (a) Ben, T.; Ren, H.; Ma, S.; Cao, D.; Lan, J.; Jing, X.; Wang, W.; Xu, J.; Deng, F.; Simmons, J. M.; Qiu, S.; Zhu, G. *Angew. Chem., Int. Ed.* **2009**, *48*, 9457. (b) Ren, H.; Ben, T.; Wang, E.; Jing, X.; Xue, M.; Liu, B.; Cui, Y.; Qiu, S.; Zhu, G. *Chem. Commun.* **2010**, *46*, 291.

(4) Sakaushi, K.; Nickerl, G.; Wisser, F. M.; Nishio-Hamane, D.; Hosono, E.; Zhou, H.; Kaskel, S.; Eckert, J. *Angew. Chem., Int. Ed.* **2012**, *51*, 7850.

(5) (a) Kaur, P.; Hupp, J. T.; Nguyen, S. T. *ACS Catalysis* **2011**, *1*, 819. (b) Zhang, Y.; Riduan, S. N.; Ying, J. Y. *Chem.—Eur. J.* **2009**, *15*, 1077. (c) Palkovits, R.; Antonietti, M.; Kuhn, P.; Thomas, A.; Schueth, F. *Angew. Chem., Int. Ed.* **2009**, *48*, 6909. (d) Kailasam, K.; Schmidt, J.; Bildirir, H.; Zhang, G.; Blechert, S.; Wang, X.; Thomas, A. *Macromol. Rapid Commun.* **2013**, *34*, 1008. (e) Schmidt, J.; Weber, J.; Epping, J. D.; Antonietti, M.; Thomas, A. *Adv. Mater.* **2009**, *21*, 702. (f) Kundu, D. S.; Schmidt, J.; Bleschke, C.; Thomas, A.; Blechert, S. *Angew. Chem., Int. Ed.* **2012**, *51*, 5456.

(6) (a) Ren, H.; Ben, T.; Sun, F.; Guo, M.; Jing, X.; Ma, H.; Cai, K.; Qiu, S.; Zhu, G. *J. Mater. Chem.* **2011**, *21*, 10348. (b) Carboni, M.; Abney, C. W.; Taylor-Pashow, K. M. L.; Vivero-Escoto, J. L.; Lin, W. *Ind. Eng. Chem. Res.* **2013**, *52*, 15187. (c) Zhang, M.; Perry, Z.; Park, J.; Zhou, H.-C. *Polymer*, **2013**, http://dx.doi.org/10.1016/j.polymer.2013.09.029; (d) Lu, W.; Sculley, J. P.; Yuan, D.; Krishna, R.; Zhou, H.-C. *J. Phys. Chem. C* **2013**, *117*, 4057. (e) Chen, Q.; Luo, M.; Hammershoej, P.; Zhou, D.; Han, Y.; Laursen, B. W.; Yan, C.-G.; Han, B.-H. *J. Am. Chem. Soc.* **2012**, *134*, 6084.

(7) (a) Schwab, M. G.; Fassbender, B.; Spiess, H. W.; Thomas, A.; Feng, X.; Muellen, K. *J. Am. Chem. Soc.* **2009**, *131*, 7216. (b) Ben, T.; Shi, K.; Cui, Y.; Pei, C.; Zuo, Y.; Guo, H.; Zhang, D.; Xu, J.; Deng, F.; Tian, Z.; Qiu, S. *J. Mater. Chem.* **2011**, *21*, 18208. (c) Liu, X.; Xu, Y.;

Jiang, D. *J. Am. Chem. Soc.* **2012**, *134*, 8738. (d) Budd, P. M.; Elabas, E. S.; Ghanem, B. S.; Makhseed, S.; McKeown, N. B.; Msayib, K. J.; Tattershall, C. E.; Wang, D. *Adv. Mater.* **2004**, *16*, 456. (e) Chen, L.; Honsho, Y.; Seki, S.; Jiang, D. *J. Am. Chem. Soc.* **2010**, *132*, 6742. (f) Bunck, D. N.; Dichtel, W. R. *Angew. Chem., Int. Ed.* **2012**, *51*, 1885. (g) Gopalakrishnan, D.; Dichtel, W. R. *J. Am. Chem. Soc.* **2013**, *135*, 8357. (h) Novotney, J. L.; Dichtel, W. R. *ACS Macro Letters* **2013**, *2*, 423. (i) Nagai, A.; Chen, X.; Feng, X.; Ding, X.; Guo, Z.; Jiang, D. *Angew. Chem., Int. Ed.* **2013**, *52*, 3770. (j) Wan, S.; Guo, J.; Kim, J.; Ihee, H.; Jiang, D. *Angew. Chem., Int. Ed.* **2008**, *47*, 8826. (k) Pandey, P.; Katsoulidis, A. P.; Eryazici, I.; Wu, Y.; Kanatzidis, M. G.; Nguyen, S. B. T. *Chem. Mater.* **2010**, *22*, 4974. (l) Luo, Y.-L.; Li, B.-Y.; Liang, L.-Y.; Tan, B.-E. *Chem. Commun.* **2011**, *47*, 7704. (m) Hasell, T.; Wood, C. D.; Clowes, R.; Jones, J. T. A.; Khimyak, Y. Z.; Adams, D. J.; Cooper, A. I. *Chem. Mater.* **2010**, *22*, 557.

(8) (a) Budd, P. M.; Ghanem, B.; Msayib, K.; McKeown, N. B.; Tattershall, C. *J. Mater. Chem.* **2003**, *13*, 2721. (b) Kou, Y.; Xu, Y.-H.; Guo, Z.-Q.; Jiang, D.-L. *Angew. Chem., Int. Ed.* **2011**, *50*, 8753. (c) Pandey, P.; Farha, O. K.; Spokoyny, A. M.; Mirkin, C. A.; Kanatzidis, M. G.; Hupp, J. T.; Nguyen, S. B. T. *J. Mater. Chem.* **2011**, *21*, 1700. (d) Rabbani, M. G.; El-Kaderi, H. M. *Chem. Mater.* **2011**, *23*, 1650. (e) Jiang, J.-X.; Wang, C.; Laybourn, A.; Hasell, T.; Clowes, R.; Khimyak, Y. Z.; Xiao, J.; Higgins, S. J.; Adams, D. J.; Cooper, A. I. *Angew. Chem., Int. Ed.* **2011**, *50*, 1072. (f) Holst, J. R.; Stockel, E.; Adams, D. J.; Cooper, A. I. *Macromolecules* **2010**, *43*, 8531.

(9) Du, X.; Sun, Y.; Tan, B.; Teng, Q.; Yao, X.; Su, C.; Wang, W. *Chem. Commun.* **2010**, *46*, 970.

(10) Ma, L.; Wanderley, M. M.; Lin, W. *ACS Catal.* **2011**, *1*, 691.

(11) Zhang, Y.; Zhang, Y.; Sun, Y. L.; Du, X.; Shi, J. Y.; Wang, W. D.; Wang, W. *Chem.—Eur. J.* **2012**, *18*, 6328.

(12) Cuadro, A. M.; Elguero, J.; Navarro, P. *Chem. Pharm. Bull.* **1985**, *33*, 2535.

(13) (a) Chouai, A.; Simanek, E. E. *J. Org. Chem.* **2008**, *73*, 2357. (b) Lai, L.-L.; Hsu, S.-J.; Hsu, H.-C.; Wang, S.-W.; Cheng, K.-L.; Chen, C.-J.; Wang, T.-H.; Hsu, H.-F. *Chem.—Eur. J.* **2012**, *18*, 6542. (c) Zhao, H.; Jin, Z.; Su, H.; Jing, X.; Sun, F.; Zhu, G. *Chem. Commun.* **2011**, *47*, 6389.

(14) (a) Ravikovitch, P. I.; Neimark, A. V. *Langmuir* **2002**, *18*, 9830. (b) Sarkisov, L.; Monson, P. A. *Langmuir* **2001**, *17*, 7600. (c) Jeromenok, J.; Weber, J. *Langmuir* **2013**, *29*, 12982.

(15) Ma, L.; Falkowski, J. M.; Abney, C.; Lin, W. *Nat. Chem.* **2010**, *2*, 838.

(16) Lee, W.; Kim, C.; Yi, J. *J. Chem. Technol. Biotechnol.* **2002**, *77*, 1255.

(17) (a) Montoya, L. A.; Pluth, M. D. *Chem. Commun.* **2012**, *48*, 4767. (b) Lin, V. S.; Chang, C. J. *Curr. Opin. Chem. Biol.* **2012**, *16*, 595. (c) Peng, H.; Chen, W.; Cheng, Y.; Hakuna, L.; Strongin, R.; Wang, B. *Sensors* **2012**, *12*, 15907. (d) Kumar, N.; Bhalla, V.; Kumar, M. *Coord. Chem. Rev.* **2013**, *257*, 2335. (e) Lippert, A. R.; New, E. J.; Chang, C. J. *J. Am. Chem. Soc.* **2011**, *133*, 10078. (f) Bae, S. K.; Heo, C. H.; Choi, D. J.; Sen, D.; Joe, E.-H.; Cho, B. R.; Kim, H. M. *J. Am. Chem. Soc.* **2013**, *135*, 9915. (g) Mao, G.-J.; Wei, T.-T.; Wang, X.-X.; Huan, S.-y.; Lu, D.-Q.; Zhang, J.; Zhang, X.-B.; Tan, W.; Shen, G.-L.; Yu, R.-Q. *Anal. Chem.* **2013**, *85*, 7875. (h) Zhang, H.; Wang, P.; Chen, G.; Cheung, H.-Y.; Sun, H. *Tetrahedron Lett.* **2013**, *54*, 4826. (i) Zheng, F.; Wen, M.; Zeng, F.; Wu, S. *Polymer* **2013**, *54*, 5691. (j) Montoya, L. A.; Pearce, T. F.; Hansen, R. J.; Zakharov, L. N.; Pluth, M. D. *J. Org. Chem.* **2013**, *78*, 6550.

(18) (a) Lo, K. K.-W.; Chan, B. T.-N.; Liu, H.-W.; Zhang, K. Y.; Li, S. P.-Y.; Tang, T. S.-M. *Chem. Commun.* **2013**, *49*, 4271. (b) Lo, K. K.-W.; Chung, C.-K.; Lee, T. K.-M.; Lui, L.-H.; Tsang, K. H.-K.; Zhu, N. *Inorg. Chem.* **2003**, *42*, 6886. (c) Li, S. P.-Y.; Lau, C. T.-S.; Louie, M.-W.; Lam, Y.-W.; Cheng, S. H.; Lo, K. K.-W. *Biomaterials* **2013**, *34*, 7519.

(19) (a) Wang, M.-S.; Guo, G.-C.; Chen, W.-T.; Xu, G.; Zhou, W.-W.; Wu, K.-J.; Huang, J.-S. *Angew. Chem., Int. Ed.* **2007**, *46*, 3909. (b) Ki, W.; Li, J. *J. Am. Chem. Soc.* **2008**, *130*, 8114. (c) Kamtekar, K. T.; Monkman, A. P.; Bryce, M. R. *Adv. Mater.* **2010**, *22*, 572. (d) Rao, X.; Huang, Q.; Yang, X.; Cui, Y.; Yang, Y.; Wu, C.; Chen, B.; Qian, G. *J. Mater. Chem.* **2012**, *22*, 3210. (e) Sava, D. F.; Rohwer, L. E. S.; Rodriguez, M. A.; Nenoff, T. M. *J. Am. Chem. Soc.* **2012**, *134*, 3983. (f) Jeon, Y. P.; Ko, Y. S.; Choo, D. C.; Kim, T. W. *J. Nanosci. Nanotechnol.* **2012**, *12*, 3611. (g) Dai, Q.; Duty, C. E.; Hu, M. Z. *Small* **2010**, *6*, 1577. (h) Wu, H.; Ying, L.; Yang, W.; Cao, Y. *Chem. Soc. Rev.* **2009**, *38*, 3391. (i) Yang, Y.; Lowry, M.; Schowalter, C. M.; Fakayode, S. O.; Escobedo, J. O.; Xu, X.; Zhang, H.; Jensen, T. J.; Fronczek, F. R.; Warner, I. M.; Strongin, R. M. *J. Am. Chem. Soc.* **2006**, *128*, 14081. (j) Su, H.-C.; Chen, H.-F.; Fang, F.-C.; Liu, C.-C.; Wu, C.-C.; Wong, K.-T.; Liu, Y.-H.; Peng, S.-M. *J. Am. Chem. Soc.* **2008**, *130*, 3413. (k) Liu, J.; Cheng, Y.; Xie, Z.; Geng, Y.; Wang, L.; Jing, X.; Wang, F. *Adv. Mater.* **2008**, *20*, 1357. (l) Park, S.; Kwon, J. E.; Kim, S. H.; Seo, J.; Chung, K.; Park, S.-Y.; Jang, D.-J.; Medina, B. M.; Gierschner, J.; Park, S. Y. *J. Am. Chem. Soc.* **2009**, *131*, 14043. (m) Abbel, R.; Grenier, C.; Pouderoijen, M. J.; Stouwdam, J. W.; Leclère, P. E. L. G.; Sijbesma, R. P.; Meijer, E. W.; Schenning, A. P. H. J. *J. Am. Chem. Soc.* **2009**, *131*, 833. (n) Nandhikonda, P.; Heagy, M. D. *Chem. Commun.* **2010**, *46*, 8002. (o) Vijayakumar, C.; Sugiyasu, K.; Takeuchi, M. *Chem. Sci.* **2011**, *2*, 291. (p) Nandhikonda, P.; Heagy, M. D. *Org. Lett.* **2010**, *12*, 4796. (q) Hsu, C.-Y.; Liu, Y.-L. *J. Colloid Interface Sci.* **2010**, *350*, 75. (r) Zhang, C.; Huang, S.; Yang, D.; Kang, X.; Shang, M.; Peng, C.; Lin, J. *J. Mater. Chem.* **2010**, *20*, 6674. (s) Karpiuk, J.; Karolak, E.; Nowacki, J. *Phys. Chem. Chem. Phys.* **2010**, *12*, 8804. (t) Varghese, R.; Wagenknecht, H.-A. *Chem.—Eur. J.* **2009**, *15*, 9307. (u) He, J.; Zeller, M.; Hunter, A. D.; Xu, Z. *J. Am. Chem. Soc.* **2012**, *134*, 1553.

(20) See http://en.wikipedia.org/wiki/CIE_1931_color_space for more details.

(21) (a) Porrès, L.; Holland, A.; Pålsson, L.-O.; Monkman, A. P.; Kemp, C.; Beeby, A. *J. Fluoresc.* **2006**, *16*, 267. (b) Pålsson, L.-O.; Monkman, A. P. *Adv. Mater.* **2002**, *14*, 757. (c) De Mello, J. C.; Wittmann, F. H.; Friend, R. H. *Adv. Mater.* **1997**, *9*, 230.

(22) Murase, N.; Li, C. *J. Lumin.* **2008**, *128*, 1896.

(23) Bowers, M. J., II; McBride, J. R.; Rosenthal, S. J. *J. Am. Chem. Soc.* **2005**, *127*, 15378.